Desalination and Water Treatment
www.deswater.com
doi: 10.5004/dwt.2022.29040

277 (2022) 287–304
November

Electrochemical degradation of 1-naphthol in organic solutions using metal oxides-based nanocomposites (NiO-CuO and MnO_2-V_2O_5) and transition metal oxides (NiO, CuO, and CoO) as nanocatalyst

Esmail Mohseni[a], Sajad Zare[b], Abdolrasoul Rahmani[c,*]

[a]*Department of Environmental Health Engineering, Faculty of Evaz Health, Larestan University of Medical Sciences, Larestan, Iran, email: mohseniesmail210@gmail.com*
[b]*Department of Occupational Health, School of Public Health, Kerman University of Medical Sciences, Kerman, Iran, email: ss_zare87@yahoo.com*
[c]*Department of Occupational Health and Safety, School of Health, Larestan University of Medical Sciences, Larestan, Iran, Phone: +982433052580; Fax:+982433052477; email: rahmaniabdolrasoul218@gmail.com*

Received 21 March 2022; Accepted 13 October 2022

ABSTRACT

The electrochemical degradation of 1-naphthol (1-N) in organic solutions (C_2H_3N, C_2H_5OH, or CH_3OH) was studied by an electrochemical method using transition metal oxides (TMO) and metal oxides-based nanocomposites (MOBNC) as nanocatalyst in the presence of copper (Cu), aluminum (Al), glassy carbon (GC), and platinum (Pt) electrodes. The TMO (CuO, NiO and CoO) and MOBNC (NiO-CuO and MnO_2-V_2O_5) nanocatalysts were synthesized by the incipient wetness impregnation method. The nanocatalyst was characterized by field-scattering scanning electron microscopy and X-ray diffraction analysis. The degradation products were identified by gas chromatograph mass spectrometer (GC-MS), $^1H/^{13}C$ nuclear magnetic resonance, Distortionless Enhancement by Polarization Transfer, and the progress in the reaction was monitored using thin-layer chromatography (TLC). The electrochemical oxidation of 1-N in organic solutions in the presence of TMO and MOBNC nanocatalysts using metal electrodes (Al-Al, Cu-Cu, Pt-Pt, Al-Cu, and Cu-Al) produced 1,4-naphthoquinone (1,4-NQ), 1,2-naphthoquinone (1,2-NQ), and di(2-ethylhexyl)phthalate (DEHP). The change of one of the electrodes to GC and Pt (Al-GC, Pt-GC, Cu-GC, Cu-Pt, Al-Pt), the lack of MOBNC and TMO NPs, and the use of non-electrochemical methods (lack of application of electrical potential) do not result in the formation of products.

Keywords: 1-Naphthol; Electrochemical degradation; Transition metal oxides (TMO); Metal oxides-based nanocomposites (MOBNC); Nanocatalyst

1. Introduction

Water and soil contamination by polycyclic aromatic hydrocarbon (PAH) compounds are among the major current environmental problems because these contaminants can easily migrate in the media and cause harmful effects to human health or ecological systems. This problem is mainly due to the contamination of water bodies with organic contaminants through the release of raw agricultural, industrial, hospital, domestic, and pharmaceutical industrial wastewater into the environment [1]. 1-Naphthol (1-N), a large-scale industrial chemical used for the production of various industrial materials such as insecticides, dyes, plastics, pharmaceuticals, rubbers, etc.,

* Corresponding author.

is a metabolite of the extensively used insecticide carbaryl (1-naphthyl-N-methylcarbamate) and is hazardous [2]. The presence of hydroxyl group (OH) in the structure of the 1-N leads to their increased solubility and portability in natural aquifers and is considered more toxic than their structurally similar PAHs. Also, it affects male reproductive health, namely serum testosterone levels, sperm motility, and sperm DNA damage [3].

Great efforts have been devoted to the removal of 1-N from the environment. Some chemical, physical, and biological processes have been developed for water and wastewater treatment. In this regard, various techniques such as ozone oxidation [4], photocatalysis [5], metal–organic frameworks (MOFs) [6], biological treatment [7], adsorption [8–10], chemical oxidation [11], and radiolysis [12] were applied for removal of 1-N from aqueous and organic solutions. But there are few sufficiently efficient processes for the removal of 1-N due to toxic nature, unavailability, produce secondary pollution, and maintenance high [13–16]. This necessitated the development of alternative technologies to efficiently remove organic pollutants from aqueous solutions to complement the existing conventional methods. In the last decades, oxidation processes based on electrochemical technology have been considerably attracted by scientists in various environmental applications.

Aromatic compounds can be effectively degraded by electrochemical reactions. In this regard, some researchers such as Santos et al. [17], Pacheco et al. [18], Zhou et al. [19], Wang et al. [20], Gao et al. [21], Yao et al. [22], and Shestakova & M. Sillanpää [23], have researched on electrodegradation of phenol, 3-amino-4-hydroxy-5-nitrobenzenesulfonic acid, benzophenone-3, enrofloxacin, methyl red, metolachlor and neutral red in aqueous and organic solutions, respectively. Electrochemical degradation methods are effective techniques and have major advantages, including high efficiency, no production of sludge during the treatment, mild reaction conditions, low cost, easy operation, quick responses, and production of final products with low toxicity or non-toxic compounds like CO_2, H_2O and NH_3 [13]. Several studies also indicated that the application of metal catalysts can accelerate the degradation of organic compounds by electrochemical oxidation, thereby producing a better efficiency process [24,25].

The removal of organic compounds via electrodegradation catalyzed by nanocatalysts has been widely developed among the chemical techniques. These nanocatalysts involving copper oxide (CuO), nickel oxide (NiO), and cobalt oxide (CoO), and their modified nanomaterials showed efficient electrocatalytic activities for the degradation of aromatic organic compounds [26]. Metal oxides-based nanocomposites (MOBNC) have been widely used in environmental electrochemistry mainly due to their exceptional mechanical properties, cheapness, and successful scale-up in the electrochemical industry [1]. Song et al. and Shi et al. reported that Pd/Fe bimetallic catalysts has high catalytic activities in the degradation of organic compounds [27,28]. McQuillan et al. [29] synthesized an Ag(I) ion catalyst for methylene blue degradation; the degradation efficiency was high and the rate of removal reached 100%.

Oxides, particularly transition metal oxides (TMO), are emerging as most suitable catalysts for a different applications including electrochemical degradation process. CuO, CoO, NiO, MnO_2 (MnO), and V_2O_5 (VO) nanoparticles (NPs), which are TMO based nanostructures, exhibit extraordinary properties that they were used in variety of applications [30]. Among various TMO, CuO nanostructure has gained sa lot of attention because it is very reactive and its high surface volume exhibits substantial applications in catalysis [31]. CoO presents a high catalytic activity in the total oxidation of various types of VOCs, but it can suffer from thermal deactivation [32]. Also, NiO in the form of NPs has great importance due to their particular magnetic, electronic properties, and catalytic properties [33]. The MnO and VO NPs are environmentally friendly, inexpensive nanocatalysts for the oxidation of various compounds [34]. In view of these findings, NiO-CuO and MnO-VO nanocomposites and NiO, CuO, and CoO NPs have been synthesized and then were used as an efficient nanocatalyst for electrodegradation of 1-N in the presence of copper (Cu), aluminum (Al), glassy carbon (GC), and platinum (Pt) electrodes from organic solutions.

2. Experimental

2.1. Chemicals

1-N ($C_{10}H_8O$), acetonitrile (C_2H_3N), ethanol (C_2H_5OH), and methanol (CH_3OH) were purchased from Sigma and were used as received. The materials used for the synthesis of MOBNC and TMO NPs and production of required solutions were cobalt chloride ($CoCl_2$), copper nitrate ($Cu(NO_3)_2$), sodium hydroxide (NaOH), lithium perchlorate ($LiClO_4$), magnesium perchlorate ($Mg(ClO_4)_2$), petroleum ether (C_6H_{14}), Vanadium (V) oxide (V_2O_5), ethyl acetate ($C_4H_8O_2$), nickel chloride ($NiCl_2$), manganese(IV) oxide (MnO_2), sodium cyanide (NaCN), and deuterated chloroform ($CDCl_3$) purchased from Merck Company (Darmstadt, Germany). All chemicals used were analytical grade and used without further purification. Solutions were prepared in water purified by a Millipore Milli-Q system; freshly prepared solutions were used for day-to-day experiments.

2.2. Nanocatalyst preparation

2.2.1. NiO-CuO nanocomposites

In this paper, NiO-CuO nanocomposite was synthesized by the incipient wetness impregnation (IWI) method and characterized by various analytical methods [35]. Initially, 2 mmol of $NiCl_2$ was added drop by drop into the water, and the mixture was placed on the digital ultrasonic cleaner CD-4820 (Codyson, China; 50 kHz, 170 W) for the salt to fully dissolve in water. Then, 2 mmol of $Cu(NO_3)_2$ was slowly added to the solvent, and the solution was again placed on the ultrasonic device to obtain a homogeneous solution. Subsequently, 1 M NaOH was added drop by drop to the solution, and the solution was placed on the ultrasonic device for 5 min for the precipitate to form completely. The obtained precipitate was filtered using a centrifugal device (at 2,800 rpm for 10 min) and was eluted 3 times with abundant distilled water. The precipitate was then dried on watch glass for 24 h at room temperature.

2.2.2. MnO-VO nanocomposites

The MnO-VO nanocomposite was prepared by the IWI method [35]. Initially, 2 mmol of V_2O_5 with 6 mmol of NaCN were dissolved into the 10 mL deionized water and heated for 5 min. Then, the above solution was placed on the ultrasonic bath cleaner (Digital Ultrasonic Cleaner CD-4820 (170 W, 50 kHz)/China) at room temperature for about 1 min. Subsequently, 2 mmol of $KMnO_4$ was added to the solution, and the solution was placed on the ultrasonic device for 5 min for the precipitate to form completely. The obtained precipitate was filtered using a centrifugal device (at 2,800 rpm for 10 min) and washed several times with abundant distilled water. The prepared nanocatalyst was then dried for 24 h at room temperature in the air.

2.2.3. TMO NPs

The TMO NPs (CuO, NiO and CoO) were synthesized by the IWI method [35]. First, 4 mmol of metal salt ($CoCl_2$, $Cu(NO_3)_2$ or $NiCl_2$) dissolved in 10 mL of deionized water and place it on an digital ultrasonic cleaner CD 4820 (170 W, 50 kHz)/China) to obtain a homogeneous solution. Then, 7 mL of 1 M NaOH was added into the solution drop by drop for 15 min until the precipitate was completely formed. The solutions were shaken at 150 rpm for 6 min at pH 7, centrifuged at 2,800 rpm for 10 min, and then the precipitate was filtered and washed with distilled water many times and dried at room temperature in the air.

2.3. Characterization

MOBNC and TMO NPs were characterized by X-ray powder diffraction (XRD) and field-emission scanning electron microscopy (FESEM) analysis. For structural analysis of the MOBNC and TMO NPs, a Philips X'Pert-MPD X-ray diffractometer (40 kV and 30 mA) was used in the diffraction angle range of 2θ = 10–70, using Cu-Kα radiation. The field-emission scanning electron microscopy (FE-SEM) images were taken by field emission scanning electron microscopy (FE-SEM; Philips XL-30) for examination of surface morphology of prepared nanocatalysts. Nuclear magnetic resonance (NMR) spectroscopy was used to identify the molecular structure of the chemical compound as well as quality control. The ^{1}H-NMR and ^{13}C-NMR spectra were recorded on a 400 MHz NMR spectrophotometer (Bruker, Billerica, MA, USA) and chemical shift (δ) values were recorded in ppm. The Distortionless Enhancement by Polarization Transfer (DEPT) techniques (Bruker, Billerica, MA, USA) used for determining the presence of primary, secondary, and tertiary carbon atoms. The degradation products were also analyzed on a gas chromatograph (HP 6890 series, Agilent Technologies, Avondale, PA) coupled to a 5973N Agilent Mass Spectrometer (Agilent Technologies, Avondale, PA, USA) and fitted with a capillary column TRB-5 (30 m × 0.25 mm × 0.25 μm).

2.4. Electrochemical reactor

The chemical oxidation of 1-N was carried out in a single-compartment electrochemical cell with a volumetric capacity of 250 mL. In an undivided glass cell, four types of electrodes, Pt, Al, GC, and Cu (thickness of 3 mm) prepared by TohoTech Company (Japan) were used as the anode and cathode with a distance of 20 mm between the two electrodes. A constant potential, 6 V DC, was applied between electrodes (PowerTech, DC Power Supply, MP3087) and operated under galvanostatic conditions at room temperature (24°C). All the reactions were carried out at constant temperature (24°C ± 0.5°C) [36].

2.5. General procedure for 1-N degradation

Tables 1 and 2 demonstrate the design of the reactions carried out for 1-N degradation using TMO and MOBNC nanocatalysts, respectively. For each experimental run, 4 mmol (0.58 g) of 1-N was dissolved in 10 mL of organic solvent (C_2H_3N, C_2H_5OH or CH_3OH) in a closed container, and 0.1 g of electrolyte ($Mg(ClO_4)_2$ or $LiClO_4$) and 0.1 mmol of nanocatalyst (CuO, NiO, CoO, MnO-VO, or NiO-CuO) was added to the solution (All experiments were repeated separately for C_2H_3N, C_2H_5OH and CH_3OH solvents). Then, the solution was introduced into the cell for 2 h (Electrochemical Reactor). The solution was agitated continuously using a magnetic stirrer to ensure adequate mixing and guarantee that sampling events were unaffected by concentration gradients (CGs) within the solution [36]. The progress in the reaction was monitored using thin-layer chromatography (TLC) on aluminum-backed Merck silica gel 60 F254 plates. To separate the products from the reacting, an organic, largely nonpolar solvent mobile phase consisting of petroleum ether-ethyl acetate solvents (2:98 v/v) was used. The above reaction was repeated and examined under different conditions for repeatability. Similarly, the blank sample was also prepared by following mentioned degradation conditions.

3. Results and discussion

3.1. Characterization

3.1.1. XRD pattern

To investigate the phase structure of nanocatalysts, the XRD spectra of the nanocomposite were taken and compared with the reference spectra from the Joint Committee on Powder Diffraction Standards (JCPDS) (Figs. 1 and 2). Fig. 1 demonstrates the XRD pattern of NiO-CuO nanocomposite and the compounds presented which are NiO and CuO NPs. As shown in Fig. 1 (NiO-CuO), the diffraction peaks obtained at 32.2°, 34.4°, 37.5°, 45.7°, and 50.7° corresponding to (110), (002), (111), (202), and (020) planes which are well matched to monoclinic CuO phase of JCPDS Card No. 89-5895 [37,38]. In the XRD pattern, compared with the standard diffraction peaks from reference the cards (JCPDS Card No. 89-7129, Ni; JCPDS Card No. 14-0481, Ni_2O_3; JCPDS Card No. 47-1049, NiO), the peaks located at 2θ values of 30°–60° can be indexed to the characteristic diffractions of NiO NPs. As can be seen from Fig. 1 (NiO-CuO), the specific peaks that appeared at 35.5°, 42.8°, and 58.1° are assigned to (111), (200), and (220) planes of cubic NiO crystallites (JCPDS Card No. 47-1049) [39]. The other sharp diffraction peaks observed at 2θ = 30.9° and 55.3° which have been identified as Ni_2O_3 NPs corresponds to (002) and (202) crystal planes, respectively (JCPDS Card

Table 1
Design of the reactions carried out for 1-N degradation using TMO nanocatalysts

No.	Primary substance	Solvent	Nanocatalyst	Salt	Cathode	Anode	Removal efficiencies
1	1-N	C_2H_3N	NiO	$Mg(ClO_4)_2$	Al	Al	95.2
2	1-N	C_2H_3N	NiO	$Mg(ClO_4)_2$	Cu	Al	97.5
3	1-N	C_2H_3N	NiO	$LiClO_4$	Al	Cu	95.6
4	1-N	C_2H_3N	NiO	$Mg(ClO_4)_2$	Al	Pt	95.1
5	1-N	C_2H_3N	NiO	$LiClO_4$	Pt	Al	95.3
6	1-N	C_2H_3N	NiO	$Mg(ClO_4)_2$	Pt	Pt	96
7	1-N	C_2H_3N	NiO	$Mg(ClO_4)_2$	Cu	Cu	99.4
8	1-N	C_2H_3N	NiO	$LiClO_4$	Pt	Cu	97.8
9	1-N	C_2H_3N	NiO	$Mg(ClO_4)_2$	Cu	Pt	98
10	1-N	C_2H_3N	NiO	$Mg(ClO_4)_2$	Al	GC	96.3
11	1-N	C_2H_3N	NiO	$Mg(ClO_4)_2$	Cu	GC	97.6
12	1-N	C_2H_3N	NiO	$Mg(ClO_4)_2$	Pt	GC	95.9
13	1-N	C_2H_3N	CuO	$Mg(ClO_4)_2$	Al	Al	97.8
14	1-N	C_2H_3N	CuO	$Mg(ClO_4)_2$	Cu	Al	98.5
15	1-N	C_2H_3N	CuO	$LiClO_4$	Al	Cu	98
16	1-N	C_2H_3N	CuO	$Mg(ClO_4)_2$	Al	Pt	97.4
17	1-N	C_2H_3N	CuO	$LiClO_4$	Pt	Al	96.2
18	1-N	C_2H_3N	CuO	$Mg(ClO_4)_2$	Pt	Pt	96
19	1-N	C_2H_3N	CuO	$Mg(ClO_4)_2$	Cu	Cu	99.8
20	1-N	C_2H_3N	CuO	$LiClO_4$	Pt	Cu	99
21	1-N	C_2H_3N	CuO	$Mg(ClO_4)_2$	Cu	Pt	99.1
22	1-N	C_2H_3N	CuO	$Mg(ClO_4)_2$	Al	GC	98.2
23	1-N	C_2H_3N	CuO	$Mg(ClO_4)_2$	Cu	GC	98.7
24	1-N	C_2H_3N	CuO	$Mg(ClO_4)_2$	Pt	GC	97.6
25	1-N	C_2H_3N	CoO	$Mg(ClO_4)_2$	Al	Al	97.66
26	1-N	C_2H_3N	CoO	$Mg(ClO_4)_2$	Cu	Al	98.9
27	1-N	C_2H_3N	CoO	$LiClO_4$	Al	Cu	98.1
28	1-N	C_2H_3N	CoO	$Mg(ClO_4)_2$	Al	Pt	96.7
29	1-N	C_2H_3N	CoO	$LiClO_4$	Pt	Al	96.6
30	1-N	C_2H_3N	CoO	$Mg(ClO_4)_2$	Pt	Pt	95.9
31	1-N	C_2H_3N	CoO	$Mg(ClO_4)_2$	Cu	Cu	98.3
32	1-N	C_2H_3N	CoO	$LiClO_4$	Pt	Cu	98
34	1-N	C_2H_3N	CoO	$Mg(ClO_4)_2$	Cu	Pt	98.4
35	1-N	C_2H_3N	CoO	$Mg(ClO_4)_2$	Al	GC	95.8
36	1-N	C_2H_3N	CoO	$Mg(ClO_4)_2$	Cu	GC	97
37	1-N	C_2H_3N	CoO	$Mg(ClO_4)_2$	Pt	GC	95.4

Notes: All the above experiments were repeated for ethanol (C_2H_5OH) and methanol (CH_3OH) solvents;
All reactions were performed under ambient atmosphere.

No. 14-0481). Furthermore, Fig. 1 (NiO-CuO) show another peaks which agreement with the reference cards (JCPDS Card No. 89-7129: cubic Ni NPs). No additional peaks were found, which means high purity of NiO-CuO composite nanocatalyst. These results are consistent with the study by Rahemi et al. [40] and Srinivasan & Punithavelan [41], who designed and fabricated a Ni-Cu/Al_2O_3 and NiO/CuO/ZnO nanocomposites, respectively.

The XRD pattern of the MnO-VO nanocomposite showed the presence of three oxides (JCPDS Card No. 41-1426, V_2O_5; JCPDS Card No. 44-0141, MnO_2; JCPDS Card No. 35-0139, MnV_2O_6) (Fig. 1. MnO-VO). Fig. 1 (MnO-VO) shows the XRD diffraction pattern of prepared α-MnO_2 NPs, which agrees with the JCPDS Card No. 44-0141. The diffraction pattern demonstrates clear peaks centered at diffraction angles (2θ°) as 28.9°, 37.7°, 48.9°, and 54.9° corresponds to (310), (211), (411), and (600) planes respectively. All the peaks in the diffraction pattern show the α-MnO_2 NPs are tetragonal crystalline structures. The peaks are well-matched with the reference data of JCPDS Card No. 44-0141 [42,43]. According to Fig. 1 (MnO-VO), the data clearly shows distinct peaks at 2θ of 15.4°, 20.4°,

Table 2
Design of the reactions carried out for 1-N degradation using MOBNC nanocatalysts

No.	Primary substance	Solvent	Nanocatalyst	Salt	Cathode	Anode	Removal efficiencies
1	1-N	C_2H_3N	MnO-VO	$Mg(ClO_4)_2$	Al	Al	99
2	1-N	C_2H_3N	MnO-VO	$Mg(ClO_4)_2$	Cu	Al	99.7
3	1-N	C_2H_3N	MnO-VO	$LiClO_4$	Al	Cu	99.5
4	1-N	C_2H_3N	MnO-VO	$Mg(ClO_4)_2$	Al	Pt	99.1
5	1-N	C_2H_3N	MnO-VO	$LiClO_4$	Pt	Al	98.7
6	1-N	C_2H_3N	MnO-VO	$Mg(ClO_4)_2$	Pt	Pt	98.9
7	1-N	C_2H_3N	MnO-VO	$Mg(ClO_4)_2$	Cu	Cu	99.8
8	1-N	C_2H_3N	MnO-VO	$LiClO_4$	Pt	Cu	99.1
9	1-N	C_2H_3N	MnO-VO	$Mg(ClO_4)_2$	Cu	Pt	99.6
10	1-N	C_2H_3N	MnO-VO	$Mg(ClO_4)_2$	Al	GC	97.9
11	1-N	C_2H_3N	MnO-VO	$Mg(ClO_4)_2$	Cu	GC	99.8
12	1-N	C_2H_3N	MnO-VO	$Mg(ClO_4)_2$	Pt	GC	98.4
13	1-N	C_2H_3N	NiO-CuO	$Mg(ClO_4)_2$	Al	Al	97.9
14	1-N	C_2H_3N	NiO-CuO	$Mg(ClO_4)_2$	Cu	Al	99.6
15	1-N	C_2H_3N	NiO-CuO	$LiClO_4$	Al	Cu	99.1
16	1-N	C_2H_3N	NiO-CuO	$Mg(ClO_4)_2$	Al	Pt	98
17	1-N	C_2H_3N	NiO-CuO	$LiClO_4$	Pt	Al	97.4
18	1-N	C_2H_3N	NiO-CuO	$Mg(ClO_4)_2$	Pt	Pt	98.8
19	1-N	C_2H_3N	NiO-CuO	$Mg(ClO_4)_2$	Cu	Cu	99.5
20	1-N	C_2H_3N	NiO-CuO	$LiClO_4$	Pt	Cu	99.7
21	1-N	C_2H_3N	NiO-CuO	$Mg(ClO_4)_2$	Cu	Pt	99.8
22	1-N	C_2H_3N	NiO-CuO	$Mg(ClO_4)_2$	Al	GC	98.2
23	1-N	C_2H_3N	NiO-CuO	$Mg(ClO_4)_2$	Cu	GC	98.8
24	1-N	C_2H_3N	NiO-CuO	$Mg(ClO_4)_2$	Pt	GC	98.3

Notes: All the above experiments were repeated for ethanol (C_2H_5OH) and methanol (CH_3OH) solvents.
All reactions were performed under ambient atmosphere.

and 21.6°. The peaks have been identified as peaks of the orthorhombic phase of V_2O_5 with various diffracting planes (200), (001), and (101) (JCPDS Card No. 41-1426, V_2O_5). The XRD pattern revealed the formation of the crystallographic structure of V_2O_5 NPs [44]. The other peaks observed at an angle (2θ) of 28.9° and 30.5° which have been identified as MnV_2O_6 attributed to (201) and (202) crystal planes, respectively (JCPDS Card No. 35-0139) [44].

Fig. 2 shows the XRD pattern of the TMO NPs. XRD pattern of TMO-based nanocatalysts exhibited the formation of cubic CoO phase crystal structure and indexed the following planes (220), (111), (311), (222), (200), (400), (422), and (511). The observed diffraction planes were well matched with the reference cards (JCPDS Card No. 42-1467, Co_3O_4; JCPDS Card No. 48-1719, CoO) (Fig. 2. CoO) [45]. Additionally, the diffraction peaks appearing at 32.9°, 34.6°, 38.3°, 45.9°, 51.2°, and 57.9° of TMO is the standard peaks of CuO NPs (JCPDS Card No. 89-5895), which corresponding to (110), (002), (111), (202), (020), and (113) crystal planes, respectively [46,47]. Moreover, the diffraction peaks appearing at 2θ values of 30–60° are the standard diffraction patterns of NiO NPs (JCPDS Card No. 14-0481, Ni_2O_3; JCPDS Card No. 89-7129, Ni; JCPDS Card No. 47-1049, NiO), which corresponding to (002), (111), (200), (111), (202), and (220) crystal faces, respectively [48–50].

3.1.2. FE-SEM image

The morphology of MOBNC nanocatalysts was assessed by FE-SEM images as shown in Fig. 3. The FE-SEM image (Fig. 3) showed tubular structure for the NiO-CuO nanocomposite. As seen from the image, nanotubes of about 40 nm in diameter and 400 nm in length were observed. As shown in Fig. 3, the MnO-VO nanocomposite was composed of three-dimensional (3D) microspheres with diameters in the range of 50 to 100 nm.

The morphology of the TMO nanocrystallites is shown in Fig. 4. As can be seen in the SEM images, the size of CuO, NiO, and CoO NPs are in the range of 10–20 nm, 70–60 nm, and 100–70 nm, respectively. It is clear from the images that the NPs were agglomerated highly in nature and have become larger due to overlapping or aggregating of smaller particles.

3.2. Degradation of 1-N

The electrochemical oxidation reaction of 1-N in solvent (C_2H_3N, C_2H_5OH or CH_3OH) in the presence of an electrolyte ($Mg(ClO_4)_2$ and $LiClO_4$) and nanocatalyst (CuO, NiO, CoO, MnO-VO, or NiO-CuO) using electrodes (Al-Al, Cu-Cu, Pt-Pt, Al-Cu, and Cu-Al) produces 1,4-naphthoquinone

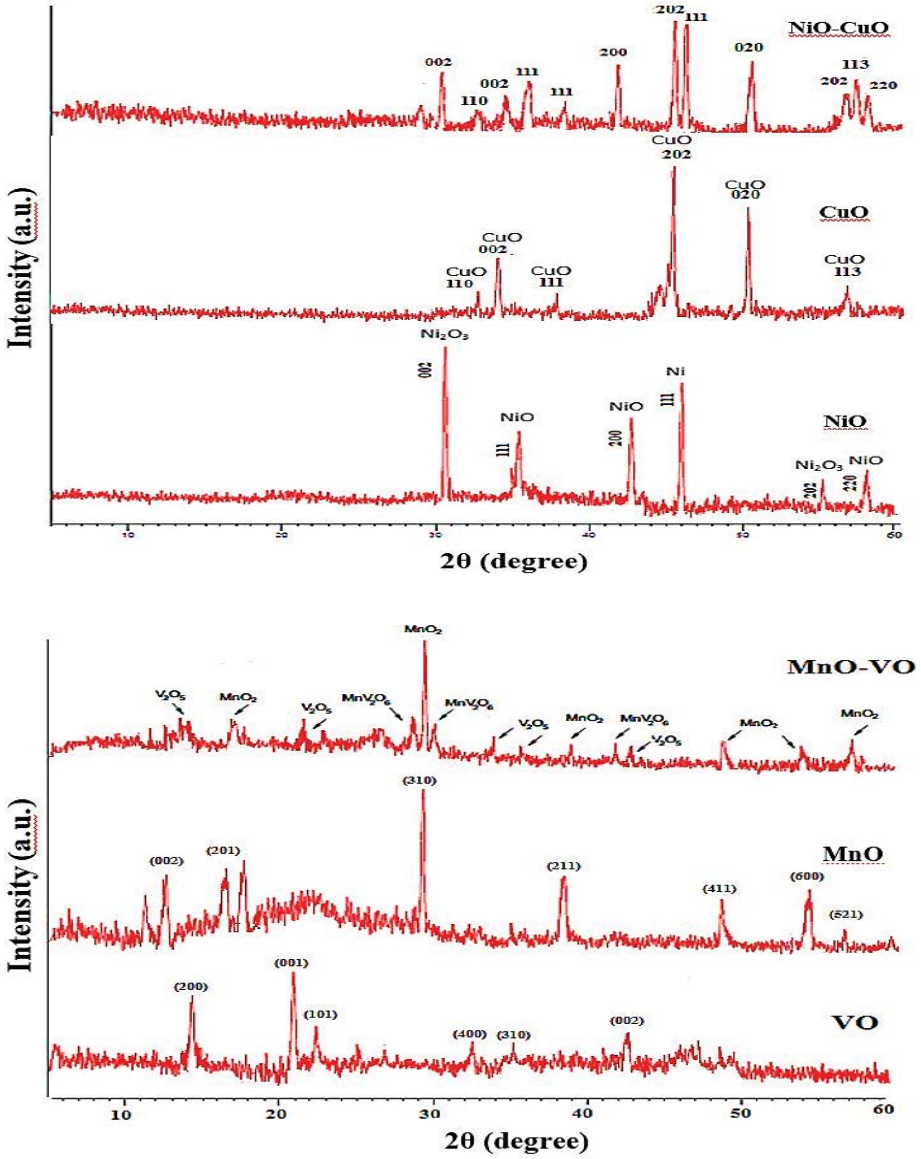

Fig. 1. XRD pattern of NiO-CuO and MnO-VO composite nanocatalysts.

(1,4-NQ), 1,2-naphthoquinone (1,2-NQ), and di(2-ethylhexyl) phthalate (DEHP). According to the product distribution and the previous research [36,46–55], the mechanism for the degradation process was described as shown in Fig. 5a–c. As can be seen in electrochemical reaction mechanisms, 1-N degradation mainly depended on direct oxidation or indirect oxidation with hydrogen peroxide (H_2O_2) and hydroxyl radical ($^{\bullet}OH$) during the electrodegradation process [36]. Anodic oxidation is the best-known direct electrochemical method, where organics are mainly destroyed by reaction with adsorbed $^{\bullet}OH$ formed at the surface of anode from water oxidation [46]. More potent indirect electro-oxidation methods for aqueous media are based on the electrogeneration of H_2O_2 [46]. Moreover, the degradation rate of 1-N with the presence of TMO and MOBNC nanocatalysts and in solution was much faster than the degradation rate of 1-N in solution, but the lack of nanocatalysts, no products were produced within 2 h. These results demonstrated that the presence of nanocatalysts increased the electrodegradation kinetics of 1-N. Therefore, it could be suggested that MOBNC and TMO NPs are excellent nanocatalysts for H_2O_2 activation and can increase the reaction speed. The results showed that 1-N was completely removed by electrodegradation after approximately 2 h.

The change of one of the electrodes to glassy carbon or platinum metals (Al-GC, Pt-GC, Cu-GC, Cu-Pt, Al-Pt), the lack of MOBNC and TMO NPs, and the use of non-electrochemical methods (lack of application of electrical potential) do not result in the formation of products. Poor oxidation for the synthesis of H_2O_2 is probably one of the reasons for the lack of product formation. In the present work, degradation products were confirmed using a sensitive gas chromatograph mass spectrometer (GC-MS) technique, NMR spectroscopy, and further confirmed by DEPT-135 experiments (Fig. 6).

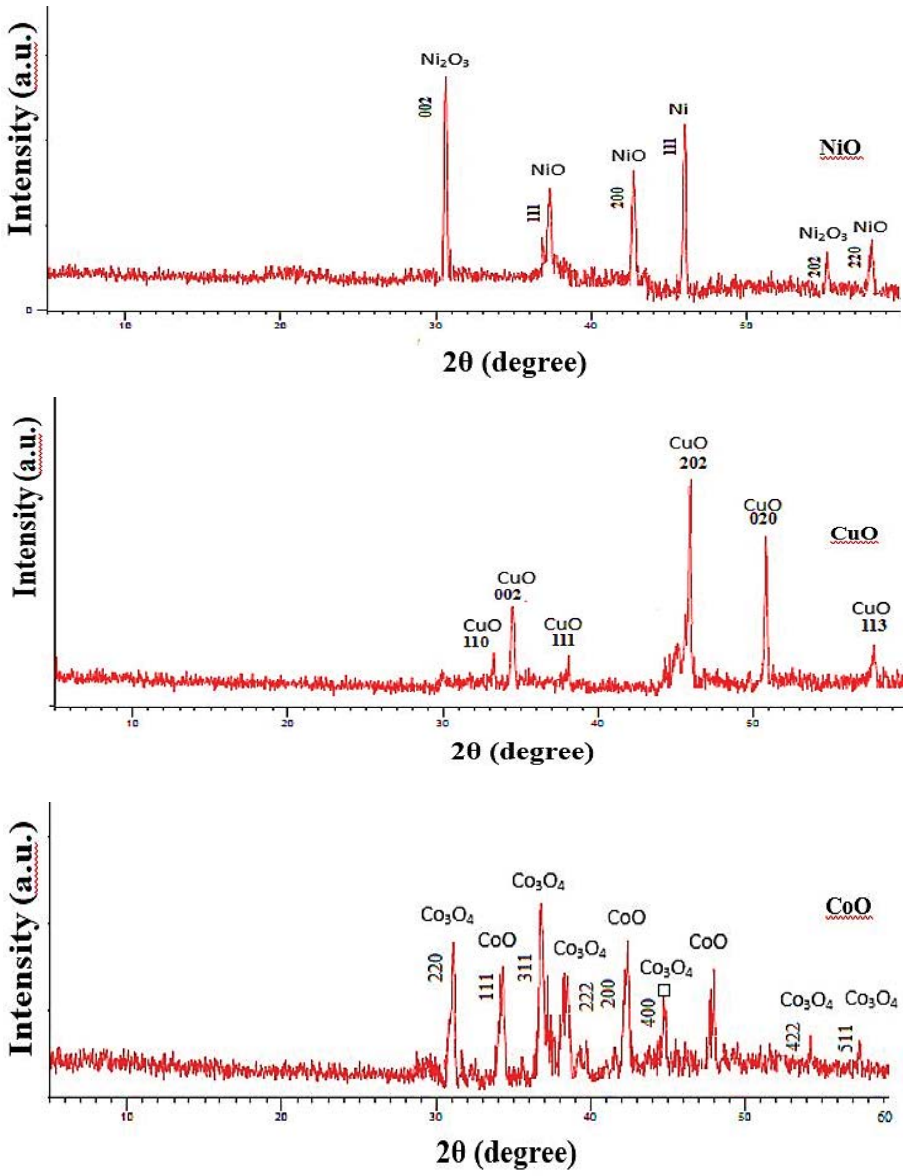

Fig. 2. XRD pattern of NiO, CuO and CoO nanocatalysts.

3.3. Structural and spectral properties

3.3.1. NMR spectral analysis

The NMR experiments and the signal assignments were made for all products. $^{1}H/^{13}C$-NMR spectra were recorded in deuterated chloroform ($CDCl_3$) by using Bruker DRX 400 Avance spectrometer and shown in Figs. 7–9.

One of the three products obtained from 1-N degradation is 1,4-NQ according to the $^{1}H/^{13}C$-NMR evidence. For 1,4-NQ, the observed values of $^{1}H/^{13}C$-NMR chemical shifts (δ) are listed in Table 3. In the present work, the ^{1}H-NMR spectrum of 1,4-NQ molecule gives different chemical shift values of the aromatic proton (protons directly attached to a benzene ring) such as 7.009, 7.8, and 8.1 ppm [47,48]. Fig. 7a illustrates the ^{1}H-NMR spectra of 1,4-NQ due to the integral of the surface below the peaks, the structure is symmetrical. The structure of the degradation products is shown in Fig. 10.

The ^{13}C-NMR spectrum of 1,4-NQ is the following (Fig. 7b): the δ 138.677 ppm is the peak associated with the carbon in the benzoquinone ring; the δ 179 ppm is associated with the carbon in the carbonyl group; and the δ 126.395–133.887 ppm range represent the peaks related to the carbon in the aromatic ring [49]. Carbonyl group carbon has the largest chemical shift, due to sp2 hybrid orbitals as well as direct connection of electronegative oxygen to carbonyl carbon. The calculated 13C chemical shift is shown in Table 3. These findings are in agreement with those obtained by Daniel and Bratt [49], who reported a ^{13}C-NMR spectra data of 1,4-NQ.

The other product obtained from 1-N degradation is 1,2-NQ according to the ^{1}H-NMR evidence (Fig. 8a and b). The ^{1}H-NMR spectrum of 1,2-NQ exhibits a chemical shift (ppm) at 7.55–8.5 range which is related to protons on the benzene ring (Table 4). Generally, aromatic protons (H on

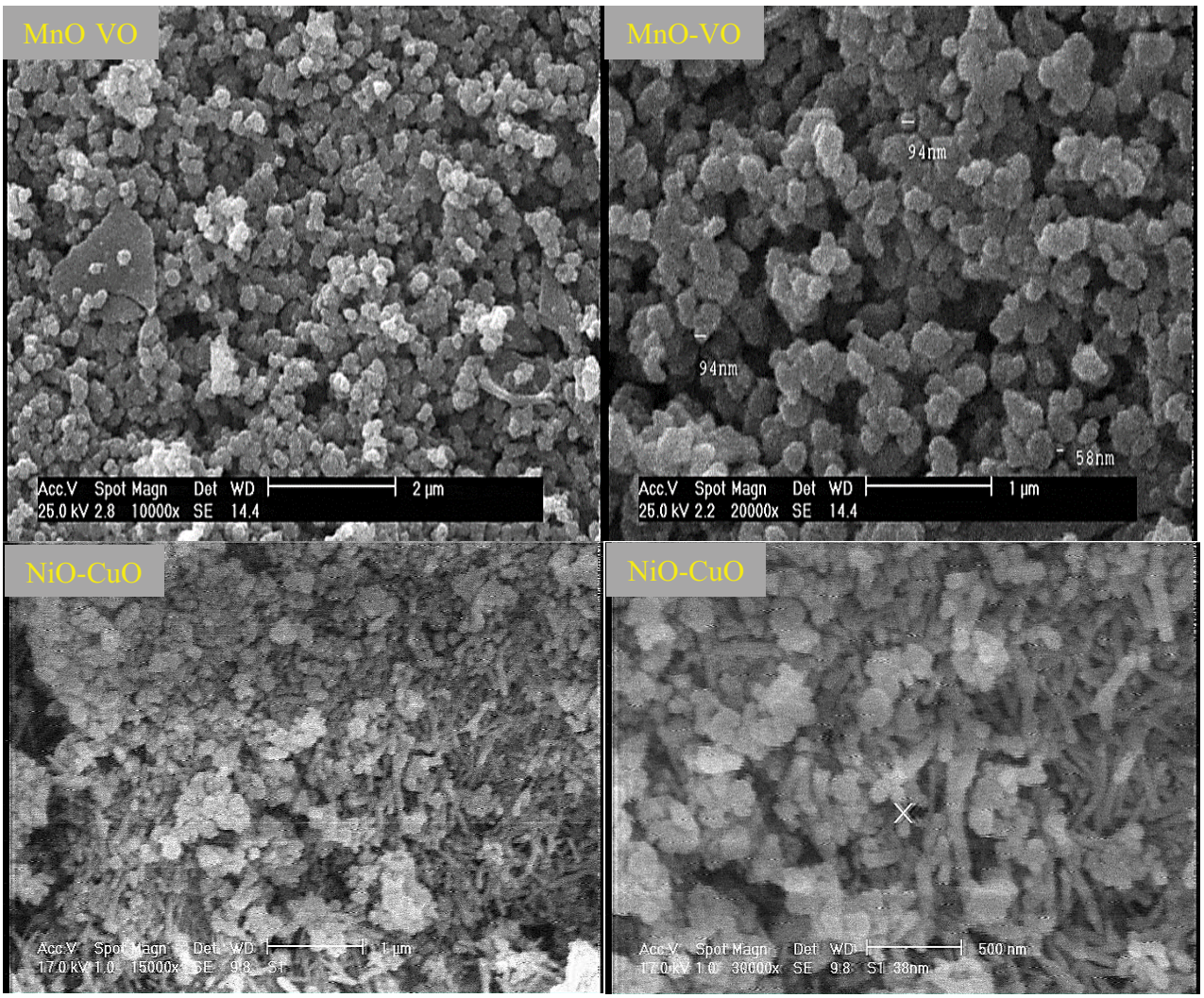

Fig. 3. FE-SEM image of NiO-CuO and MnO-VO composite nanocatalysts.

benzene ring) are strongly de-shielded, due to the anisotropy of the induced field produced by the circulation of electrons in the π bond. Their chemical shift is far downfield, in the range of 6.5–8.5 ppm [49].

By comparison of $^{1}H/^{13}C$-NMR data to those published in the literature [50–56], the other product of the degradation process was identified as DEHP. Fig. 9a and Table 5 shows ^{1}H-NMR signals of DEHP with their chemical shifts and their assignments to protons of the different functional groups. For ^{1}H-NMR, chemical shifts at 0.9 ppm, 1.35–1.43 ppm, 1.7 ppm, 4.19–4.28 ppm, and 7.5–7.7 ppm can be attributed to methyl group, methylene group, tertiary alkyl group, methane group, and aromatic protons, respectively [50–56].

The chemical shifts (ppm) of the ^{13}C-NMR are 10.96–14.05, 22.98–30.36, 68.15, 128.80–132.45 and 167 can be related to signals of methyl group, ethyl group, acetate group, aromatic ring, and carbonyl group, respectively (Fig. 9b), which are fully identical to the structure of DEHP [49–55]. The resonance signals of aromatic ring carbons appear in the 128–132 ppm range as shown in Fig. 9b. The distribution of the shifts is summarized in Table 5.

The molecular formula was further confirmed by the DEPT-135 (400 MHz, CDCl3) spectrum (Fig. 11). DEPT-135 spectra showed signals of the methyl group of the main branch, the methyl group of the side branch, ethyl group of the side branch, ethyl group of the main branch, the carbon atom of the main ring directly attached to the side branch, carbon atom attached to acetate group, and the carbon atom of the aromatic ring at δ 14.057 ppm, δ 10.964 ppm, δ 22.989 ppm, δ 28.926–30.360 ppm, δ 38.72 ppm, δ 68.156 ppm, and δ 128.804–132.451 ppm, respectively [50–56]. The results are shown in Table 5 and Fig. 11. By comparison with published reports (Lotfy et al. [56], Jalil and Fakhre [57], Sani and Pateh [58]), product 3 was identified as DEHP. This is the first report for 1-N electrodegradation from aqueous solutions.

3.3.2. GC/MS analysis

The products of electrocatalytic degradation of 1-N (see spectra in Fig. 12) were also analyzed by using Hewlett Packard (HP) 6890 gas chromatograph fitted to an HP 5973 mass spectrometer. Exact mass measurements

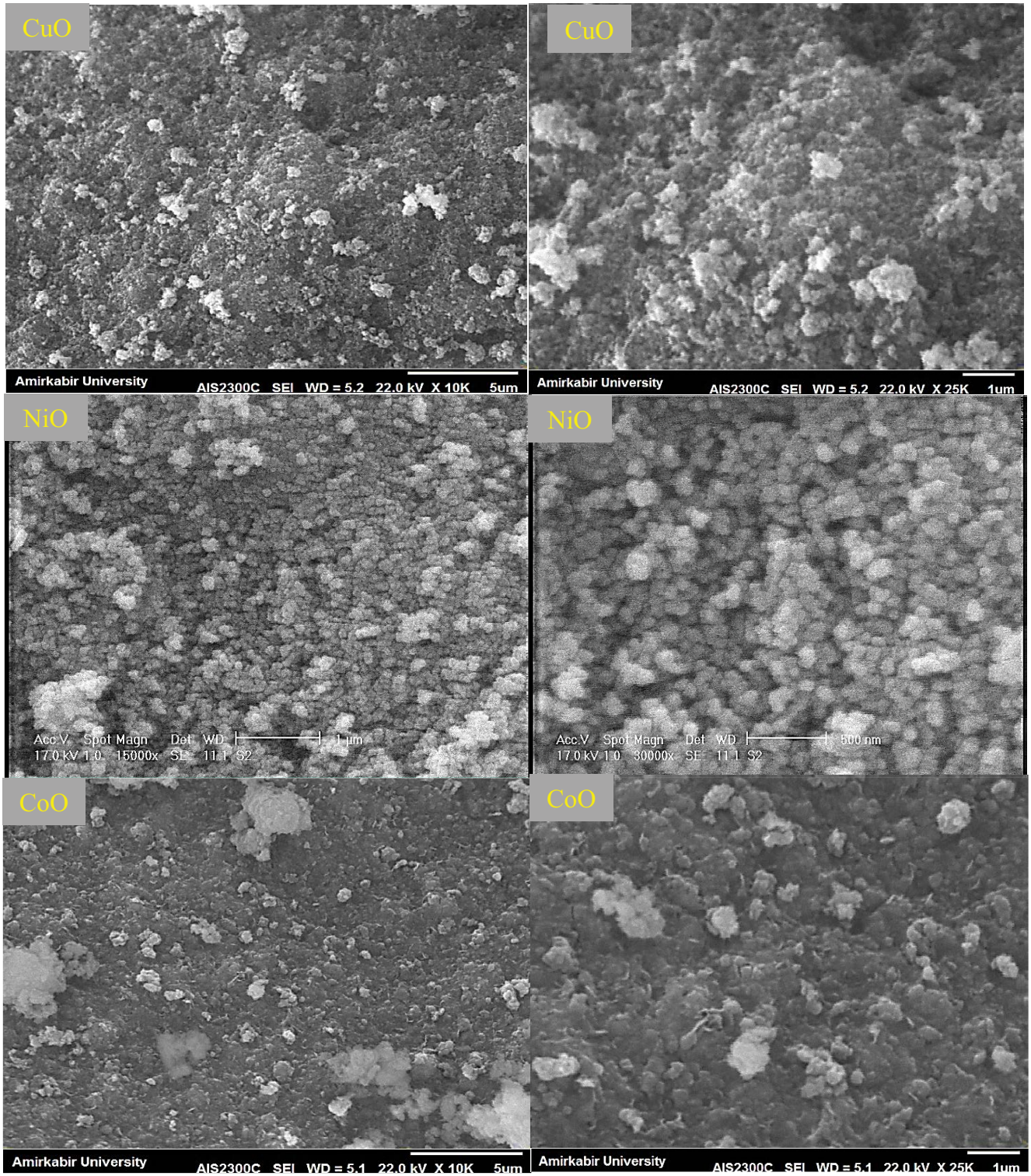

Fig. 4. FE-SEM image of CuO, NiO and CoO nanocatalysts.

of the products allowed the elemental formula of the molecules to be determined confidently. Fig. 12 shows the GC/MS chromatogram of degradation products after 3 min of irradiation. The fragment ion peaks at *m*/*z* 149 (base peak) and 167 are considered characteristic of alkyl phthalates and ions at *m*/*z* 279 and 261 suggested that the alkyl phthalate is DEHP [59]. These ion structures have been reported in a previous study and confirmed by library searching [59–61]. The structure of the ion at *m*/*z* 149, 167, and 279 are shown in Fig. 13. Since the 1-N peak

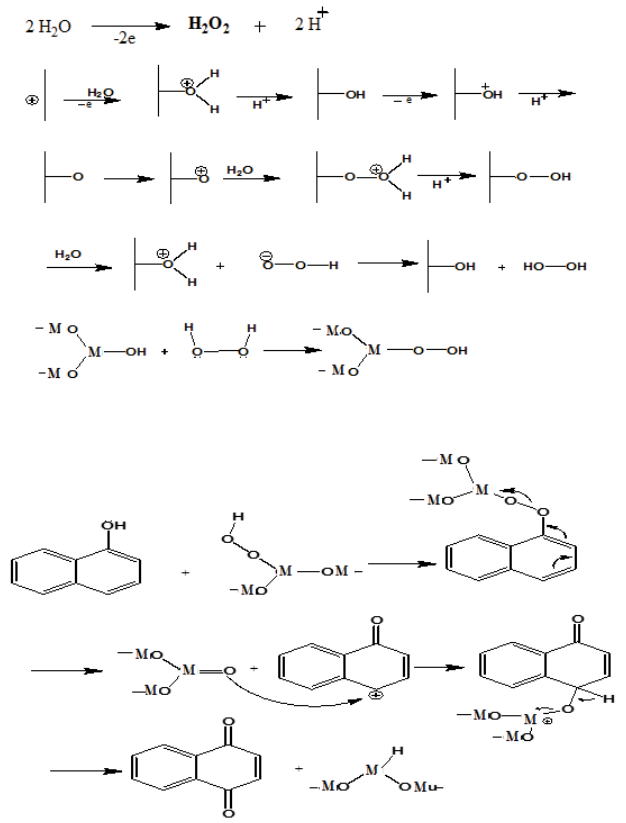

(a)

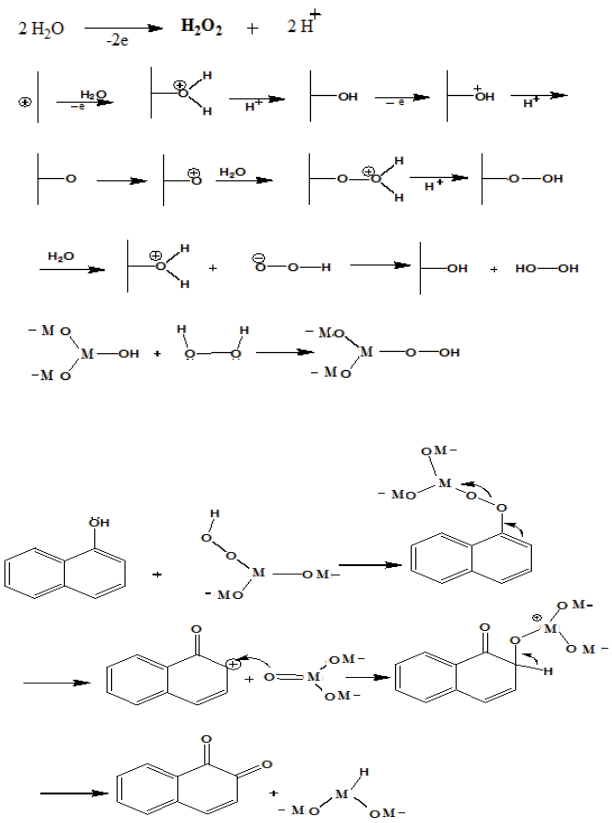

(b)

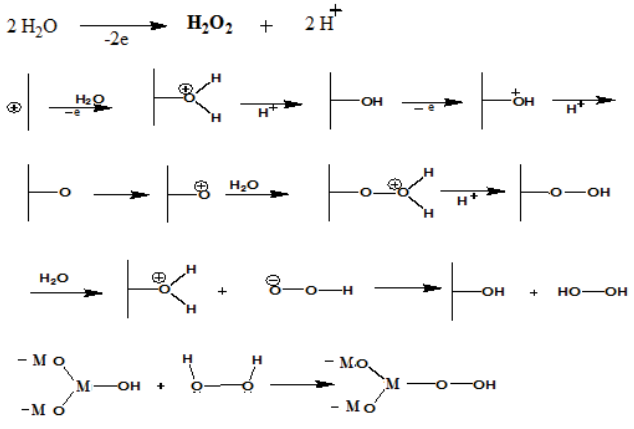

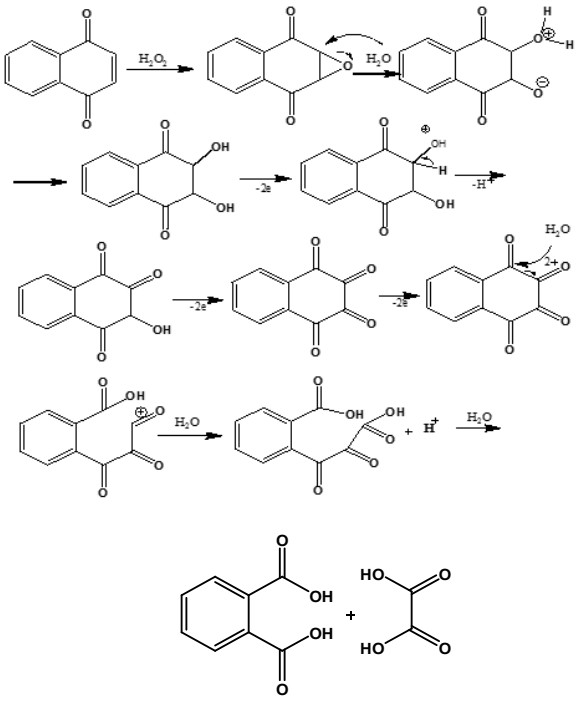

Fig. 5. *Continued*

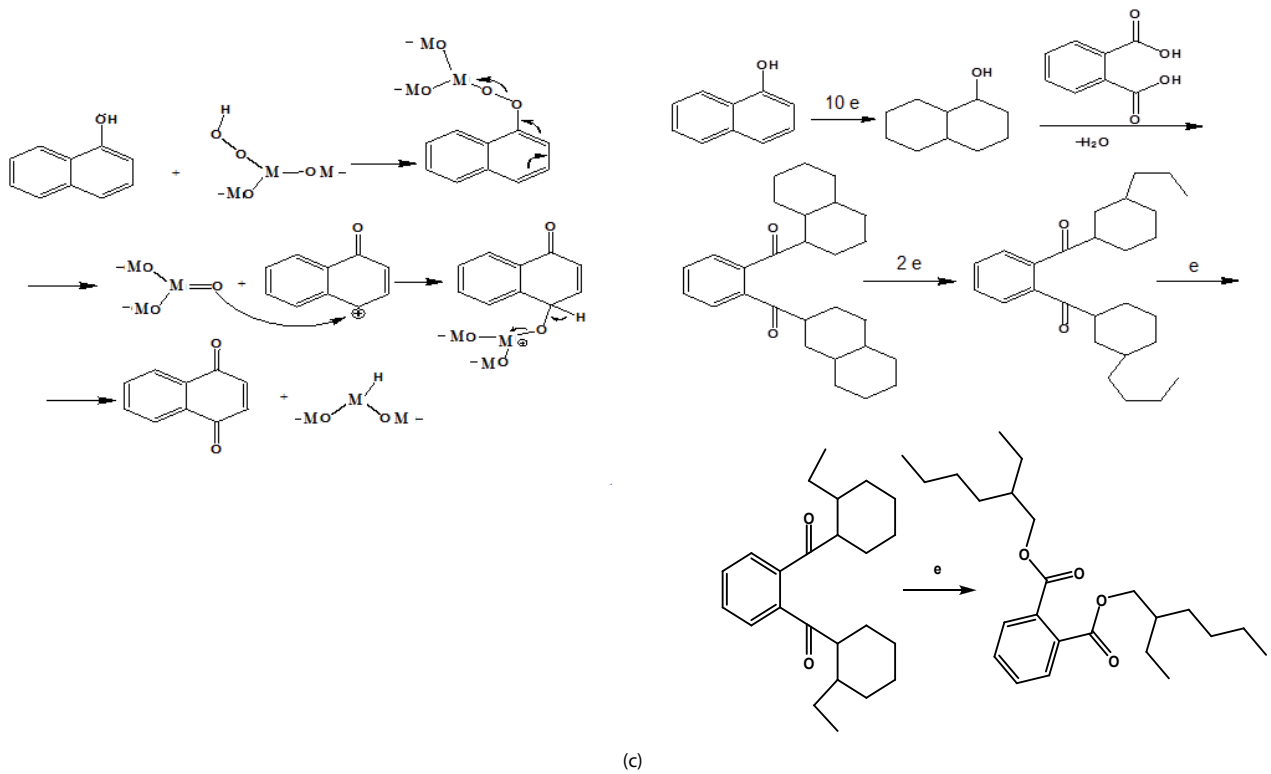

(c)

Fig. 5. Proposed mechanism for 1-N degradation and generation of (a) 1,4-NQ, (b) 1,2-NQ, and (c) DEHP.

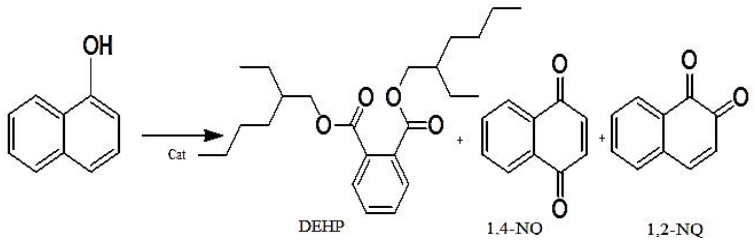

Fig. 6. Products of 1-N degradation.

Table 3
$^{1}H/^{13}C$-NMR data of 1,4-NQ

Carbon	δC	δ_H
$C_{a,b}$	133.887	7.8 (j = 3.2, CH, m)
$C_{c,d}$	126.395	8.1 (j = 3.22, CH, m)
$C_{e,f}$	129	
$C_{g,h}$	179	
$C_{i,j}$	138.677	7.009 (j = 3.2, CH, s)

Multiplicity and coupling constant (j = Hz) are in parentheses.

is not seen in the mass spectrum (144 m/z), the pollutant has been almost completely converted into products and intermediates. Phthalic acid product is a stable intermediate that is formed as a side product. Also, according to the proposed mechanism, another side product is isobenzofuran derivatives, which is obtained during the reaction from the compound of phthalic acid.

Table 4
^{1}H-NMR data of 1,2-NQ

Carbon	δ_H
C_a	7.96 (j = 8, CH, d)
C_b	7.67 (j = 8, CH, m)
C_c	7.55 (j = 8, CH, m)
C_d	7.83 (j = 8, CH, d)
C_e	8.50 (j = 8.4, CH, d)
C_f	8.021 (j = 8.4, CH, d)

Multiplicity and coupling constant (j = Hz) are in parentheses.

4. Conclusion

The TMO and MOBNC NPs as nanocatalysts were prepared by the incipient wetness impregnation method. FE-SEM indicated the morphology and surface structure of nanocatalysts. XRD distinctively recognized the presence

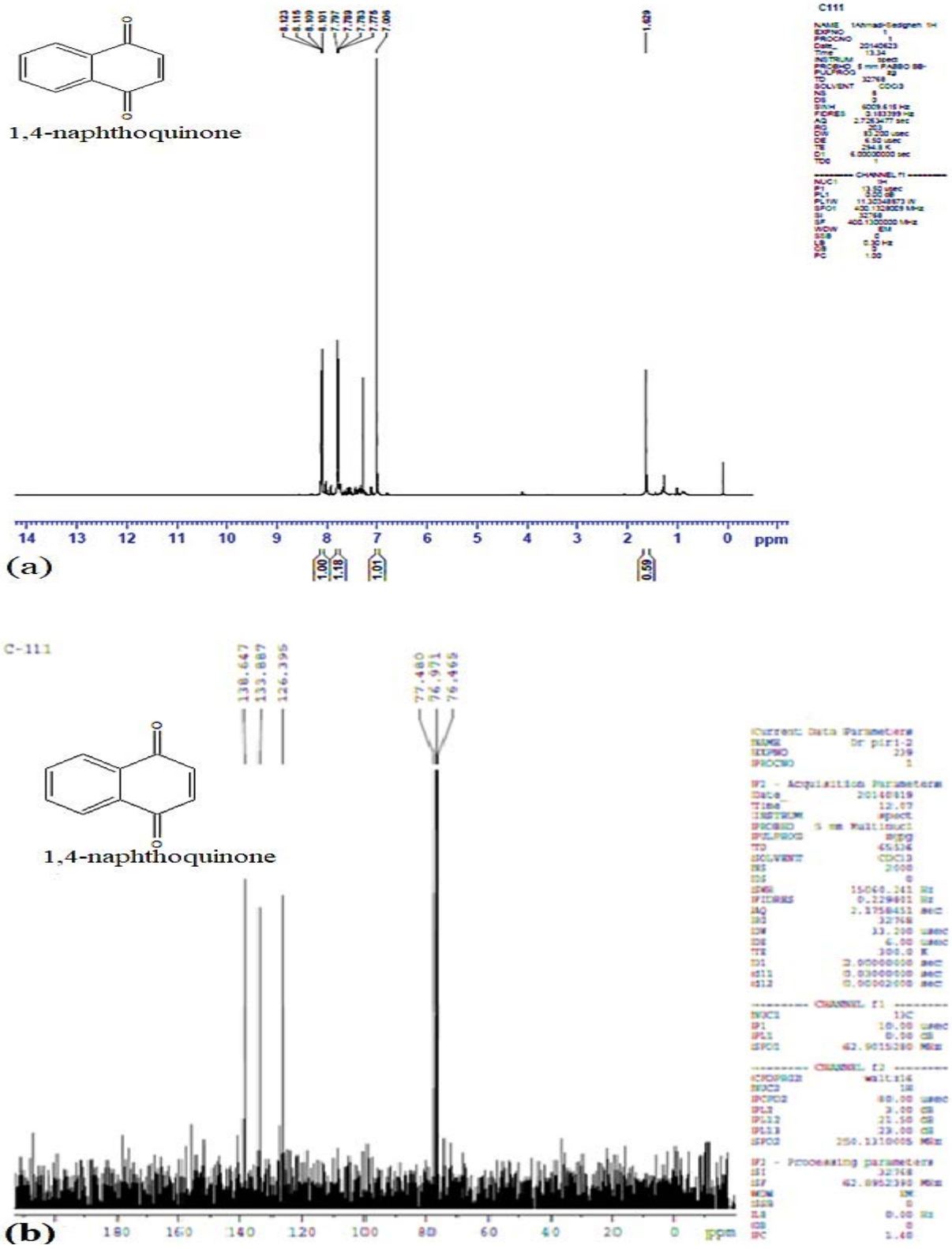

Fig. 7. [1]H-NMR spectrum (a) and [13]C-NMR spectrum (b) of 1,4-NQ.

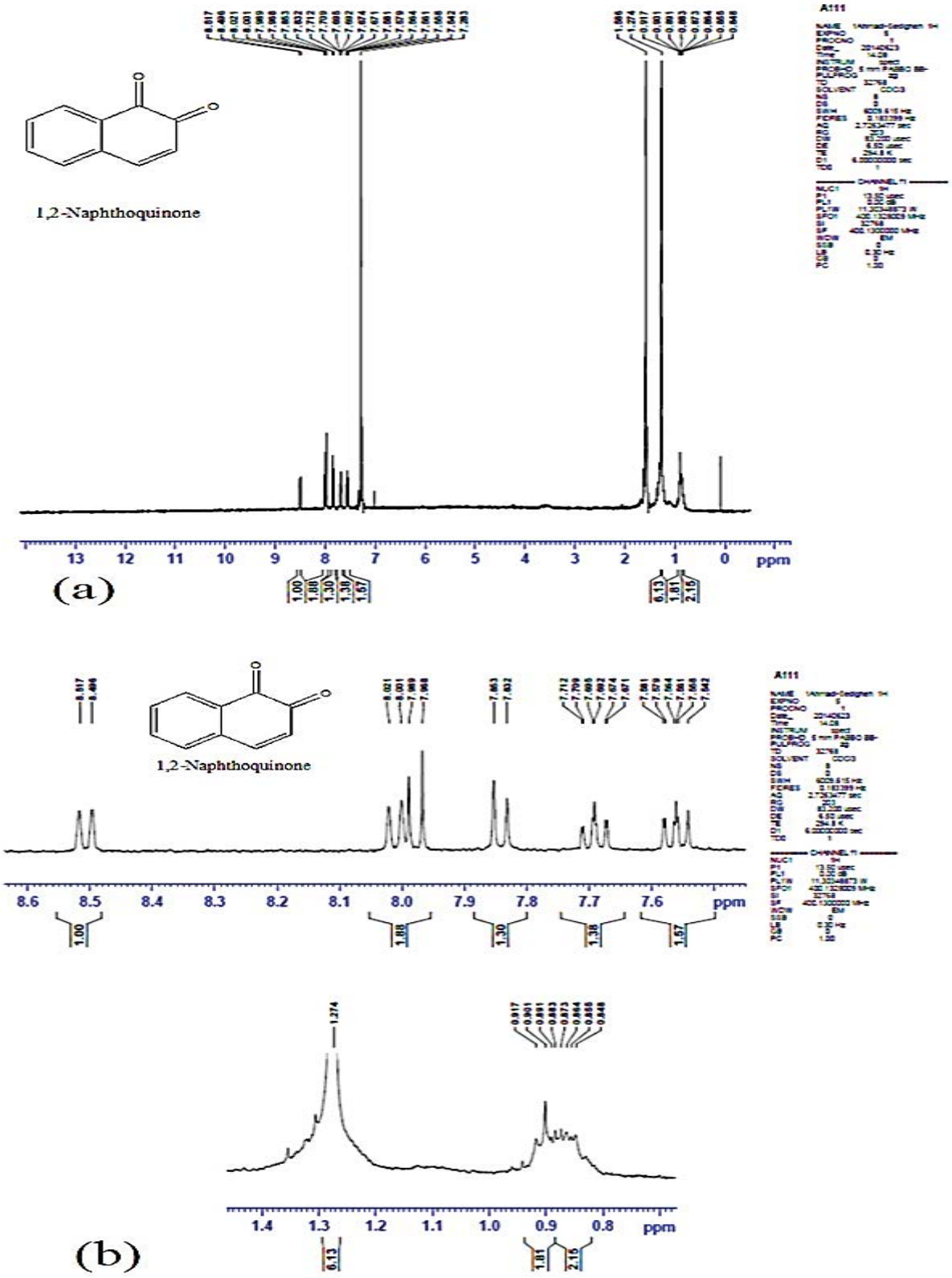

Fig. 8. ^{1}H-NMR spectrum (a) and expanded ^{1}H-NMR (b) spectrum of 1,2-NQ.

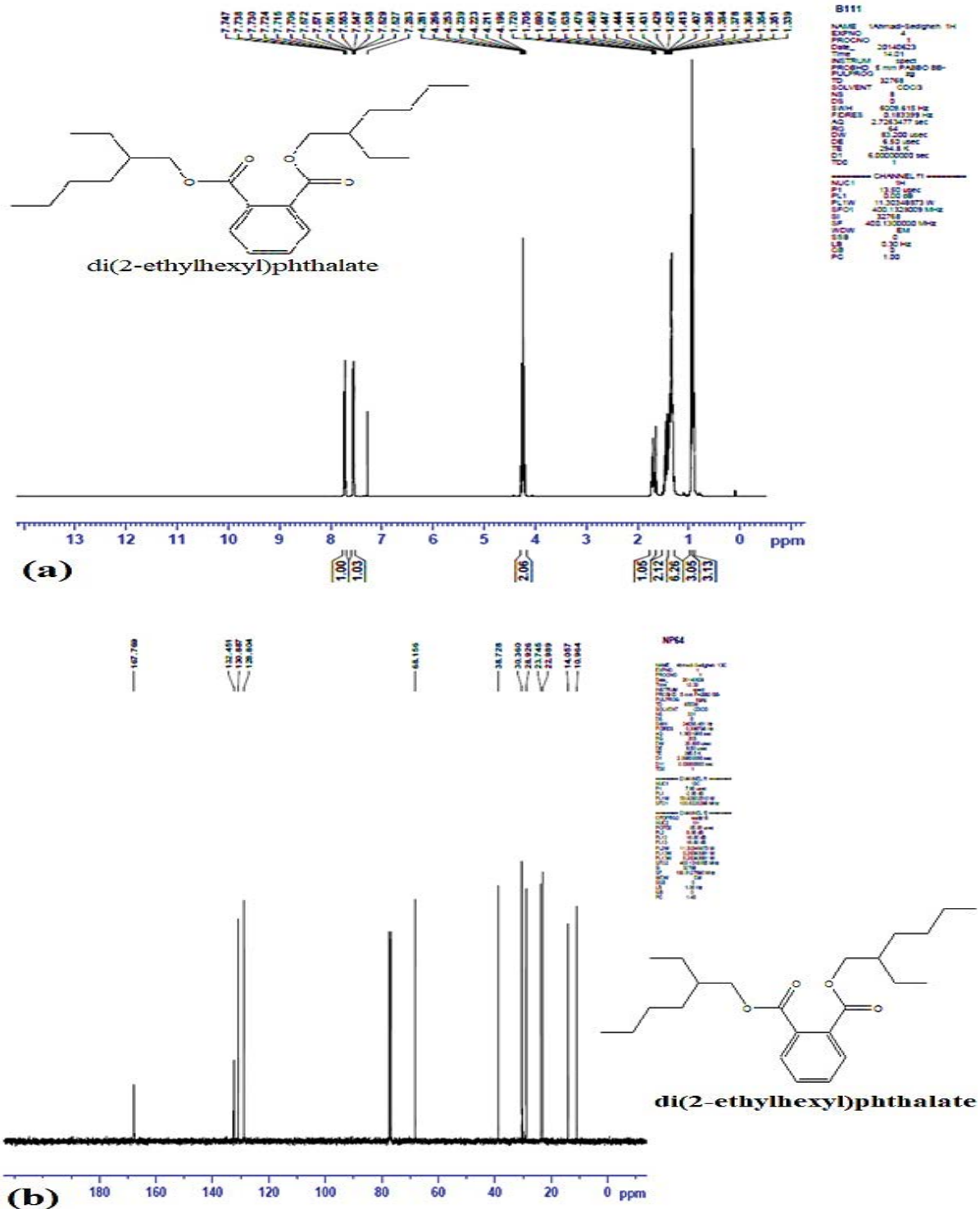

Fig. 9. ^{1}H-NMR spectrum (a) and ^{13}C-NMR spectrum (b) of DEHP.

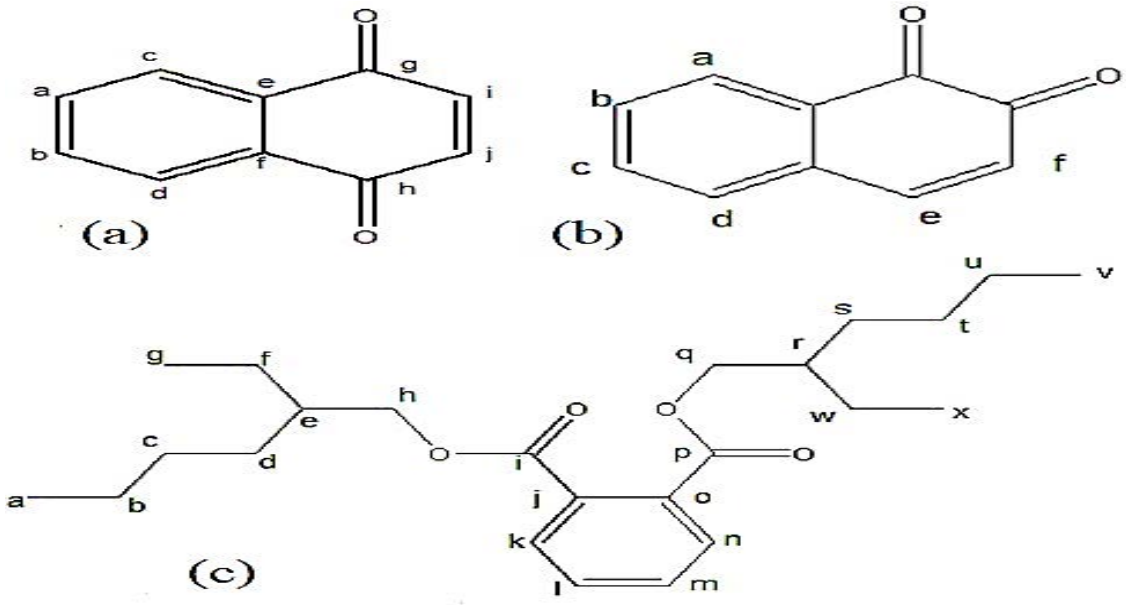

Fig. 10. Structure of 1,4-NQ (a), 1,2-NQ (b) and DEHP (c).

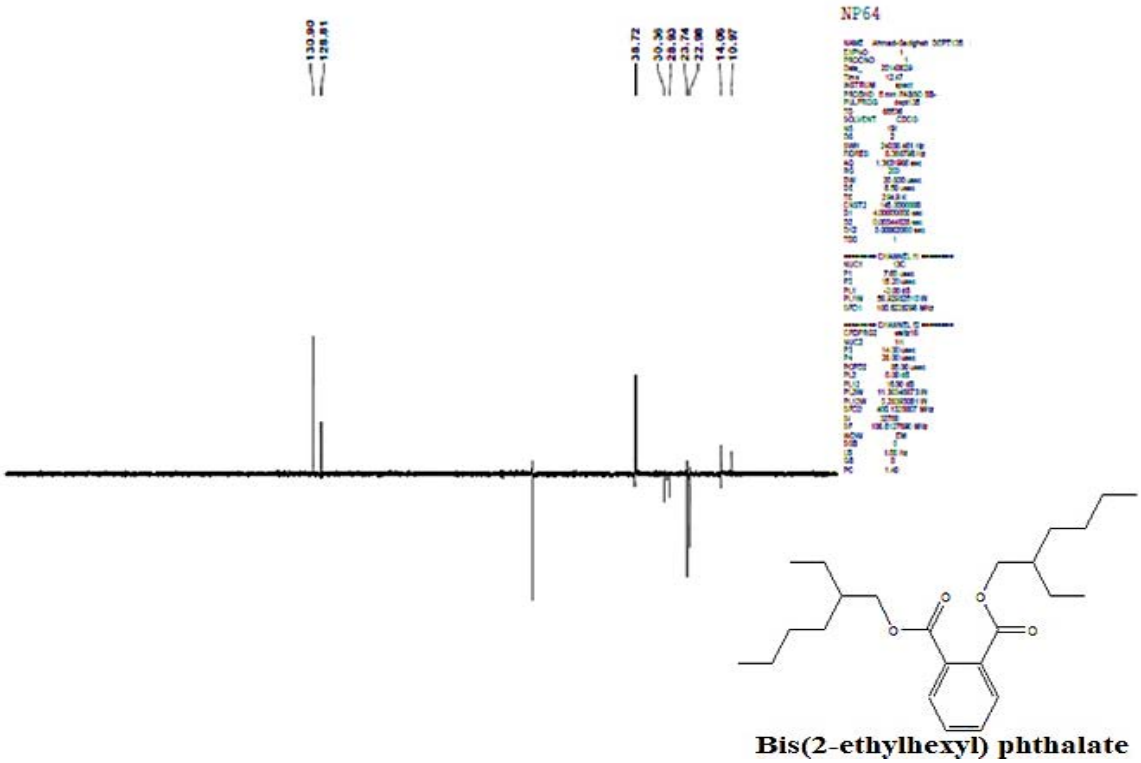

Fig. 11. DEPT-135 spectrum of DEHP.

of crystalline structures of MnO-VO, NiO-CuO, CuO, NiO, and CoO NPs. In the present work, the experimental design was carried out using the electrochemical method to investigate the 1-N degradation from an organic solution (C_2H_3N, C_2H_5OH, or CH_3OH) using TMO and MOBNC nanocatalysts and with the presence of Cu, Al, GC, and Pt electrodes. The major degradation products, 1,4-NQ, 1,2-NQ, and DEHP were identified by $^1H/^{13}C$-NMR, DEPT-135, and GC-MS techniques. Satisfactory results were obtained with effective removal of 1-N in the range of 95%–100% in the organic solutions. In accordance with the findings of the present study, the change of one of the electrodes to Al-GC, Pt-GC, Cu-GC, Cu-Pt, and Al-Pt, the lack of MOBNC and TMO nanocatalysts, and the use of non-electrochemical methods (lack of

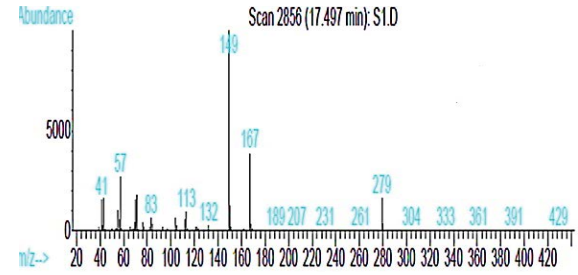

Fig. 12. Mass spectra of degradation products.

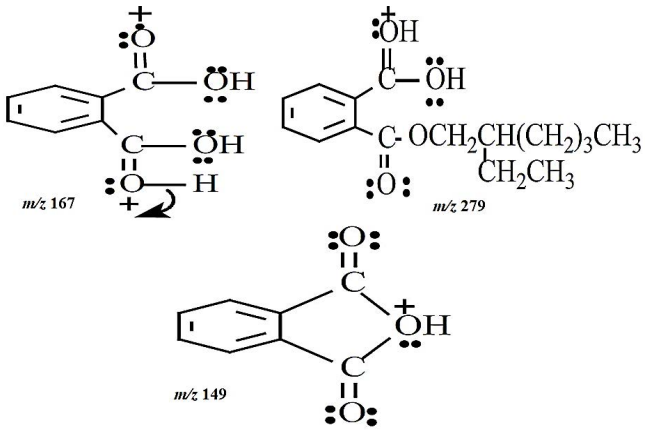

Fig. 13. Proposed structures for fragment ions at *m*/*z* 149, 167, and 279

Table 5
$^{1}H/^{13}C$-NMR and DEPT-135 data of DEHP

Carbon	δ_C	δ_H	DEPT
$C_{a,v}$	14.057	0.90 (CH_3, *t*)	14.057 (CH_3)
$C_{b,u}$	23.745	1.38 (CH_2, *m*)	23.745 (CH_2)
$C_{c,t}$	28.926	1.35 (CH_2, *m*)	28.926 (CH_2)
$C_{d,s}$	28.926	1.35 (CH_2, *t*)	28.926 (CH_2)
$C_{e,r}$	38.72	1.7 (CH, *m*)	38.72 (CH)
$C_{f,w}$	22.989	1.431 (CH_2, *t*)	22.989 (CH_2)
$C_{g,x}$	10.964	0.90 (CH_3, *t*)	10.964 (CH_3)
$C_{h,q}$	68.56	4.28, 4.196 (j = 11, 6, CH_2, *m*)	68.56 (CH_2)
$C_{i,p}$	167.7		
$C_{j,o}$	130.887		
$C_{k,n}$	18.804	7.7 (j = 5.6, CH, *m*)	128.804 (CH)
$C_{m,l}$	132.451	7.54 (j = 4, CH, *m*)	132.451 (CH)

application of electrical potential) do not result in the formation of products. Any 1-N removal under these experimental conditions may be due to direct oxidation (direct electron transfer at the anode) or reactions with •OH at the anodic surface. Such radicals are formed at the anode during the dissociation of water and are capable of fully mineralizing a variety of organic compounds. Electrochemical oxidation process for degradation of 1-N using TMO and MOBNC nanocatalysts and with the presence of metal electrodes gave substantially good results.

Funding

This research did not receive any specific grant from funding agencies in the public, commercial, or not-for-profit sectors.

Conflict of interests

The authors declare that they have no competing interests

Data availability

All necessary data are present within the manuscript.

References

[1] A.T. Lima, P.J. Kleingeld, K. Heister, J.P.G. Loch, In situ electro-osmotic cleanup of tar contaminated soil—removal of polycyclic aromatic hydrocarbons, Electrochim. Acta, 86 (2012) 142–147.
[2] X. Yan, X. Hu, T. Chen, S. Zhang, M. Zhou, Adsorptive removal of 1-naphthol from water with Zeolitic imidazolate framework-67, J. Phys. Chem. Solids, 107 (2017) 50–54.
[3] J.D. Meeker, D.B. Barr, B. Serdar, S.M. Rappaport, R. Hauser, Utility of urinary 1-naphthol and 2-naphthol levels to assess environmental carbaryl and naphthalene exposure in an epidemiology study, J. Exposure Sci. Environ. Epidemiol., 17 (2007) 314–320.
[4] X. Wang, C. Chen, J. Li, X. Wang, Ozone degradation of 1-naphthol on multiwalled carbon nanotubes/iron oxides and recycling of the adsorbent, Chem. Eng. J., 262 (2015) 1303–1310.
[5] C. Karunakaran, S. Narayanan, P. Gomathisankar, Photocatalytic degradation of 1-naphthol by oxide ceramics with added bacterial disinfection, J. Hazard. Mater., 181 (2010) 708–715.
[6] J. Lee, O.K. Farha, J. Roberts, K.A. Scheidt, S.T. Nguyen, J.T. Hupp, Metal–organic framework materials as catalysts, Chem. Soc. Rev., 38 (2009) 1450–1459.
[7] X. Yang, Y. Zhang, L. Wang, L. Cao, K. Li, A. Hursthouse, Preparation of a thermally modified diatomite and a removal mechanism for 1-naphthol from solution, Water, 9 (2017) 651, doi: 10.3390/w9090651.
[8] X. Yan, X. Hu, T. Chen, S. Zhang, M. Zhou, Adsorptive removal of 1-naphthol from water with Zeolitic imidazolate framework-67, J. Phys. Chem. Solids, 107 (2017) 50–54.
[9] H. Zheng, Y. Gao, K. Zhu, Q. Wang, M. Wakeel, A. Wahid, N.S. Alharbi, C. Chen, Investigation of the adsorption mechanisms of Pb(II) and 1-naphthol by β-cyclodextrin modified graphene oxide nanosheets from aqueous solution, J. Colloid Interface Sci., 530 (2018) 154–162.
[10] Q. Zhou, Y. Wang, J. Xiao, H. Fan, Adsorption and removal of bisphenol A, α-naphthol and β-naphthol from aqueous solution by Fe_3O_4@polyaniline core–shell nanomaterials, Synth. Met., 212 (2016) 113–122.
[11] R. Sreekanth, K.P. Prasanthkumar, M.M. Sunil Paul, U.K. Aravind, C.T. Aravindakumar, Oxidation reactions of 1- and 2-naphthols: an experimental and theoretical study, J. Phys. Chem. A, 117 (2013) 11261–11270.
[12] T. Ngo, N. Hoang, T. Tran, Radiolysis of 1-naphthol in aqueous solutions, J. Radioanal. Nucl. Chem., 286 (2010) 287–293.
[13] M. Harsini, Y.G.Y. Suyanto, L. Rhodifasari, H. Darmokoesomo, Electrochemical degradation of naphtol AS-BO batik dyes, J. Chem. Technol. Metall., 52 (2017) 1116–1122.
[14] F. Xu, D.E. Koch, I.C. Kong, R.P. Hunter, A. Bhandari, Peroxidase-mediated oxidative coupling of 1-naphthol: characterization of polymerization products, Water Res., 39 (2005) 2358–2368.
[15] X. Wang, C. Chen, J. Li, X. Wang, Ozone degradation of 1-naphthol on multiwalled carbon nanotubes/iron oxides and recycling of the adsorbent, Chem. Eng. J., 262 (2015) 1303–1310.

[16] X. Yan, X. Hu, T. Chen, S. Zhang, M. Zhou, Adsorptive removal of 1-naphthol from water with Zeolitic imidazolate framework-67, J. Phys. Chem. Solids, 107 (2017) 50–54.
[17] M.J. Santos, M.C. Medeiros, T.M. Oliveira, C.C. Morais, S.E. Mazzetto, C.A. Martínez-Huitle, S.S. Castro, Electro-oxidation of cardanol on mixed metal oxide (RuO_2-TiO_2 and IrO_2-RuO_2-TiO_2) coated titanium anodes: insights into recalcitrant phenolic compounds, Electrochim. Acta, 212 (2016) 95–101.
[18] M.J. Pacheco, V. Santos, L. Ciríaco, A. Lopes, Electrochemical degradation of aromatic amines on BDD electrodes, J. Hazard. Mater., 186 (2011) 1033–1041.
[19] C. Zhou, Y. Wang, J. Chen, J. Niu, Electrochemical degradation of sunscreen agent benzophenone-3 and its metabolite by Ti/SnO_2-Sb/Ce-PbO_2 anode: kinetics, mechanism, toxicity and energy consumption, Sci. Total Environ., 688 (2019) 75–82.
[20] C. Wang, L. Yin, Z. Xu, J. Niu, L.A. Hou, Electrochemical degradation of enrofloxacin by lead dioxide anode: kinetics, mechanism and toxicity evaluation, Chem. Eng. J., 326 (2017) 911–920.
[21] S. Gao, Y. Chen, J. Su, M. Wang, X. Wei, T. Jiang, Z.L. Wang, Triboelectric nanogenerator powered electrochemical degradation of organic pollutant using Pt-free carbon materials, ACS Nano, 11 (2017) 3965–3972.
[22] Y. Yao, G. Teng, Y. Yang, B. Ren, L. Cui, Electrochemical degradation of neutral red on PbO_2/α-Al_2O_3 composite electrodes: electrode characterization, by-products and degradation mechanism, Sep. Purif. Technol., 227 (2019) 115684, doi: 10.1016/j.seppur.2019.115684.
[23] M. Shestakova, M. Sillanpää, Electrode materials used for electrochemical oxidation of organic compounds in wastewater, Rev. Environ. Sci. Biotechnol., 16 (2017) 223–238.
[24] L. Zhou, W. Song, Z. Chen, G. Yin, Degradation of organic pollutants in wastewater by bicarbonate-activated hydrogen peroxide with a supported cobalt catalyst, Environ. Sci. Technol., 47 (2013) 3833–3839.
[25] A. Yaqub, M.H. Isa, H. Ajab, Electrochemical degradation of polycyclic aromatic hydrocarbons in synthetic solution and produced water using a Ti/SnO_2-Sb_2O_5-RuO_2 anode, J. Environ. Eng., 141 (2015) 04014074, doi: 10.1061/(ASCE) EE.1943-7870.0000900.
[26] X. Song, Q. Shi, H. Wang, S. Liu, C. Tai, Z. Bian, Preparation of Pd-Fe/graphene catalysts by photocatalytic reduction with enhanced electrochemical oxidation-reduction properties for chlorophenols, Appl. Catal., B, 203 (2017) 442–451.
[27] Q. Shi, H. Wang, S. Liu, L. Pang, Z. Bian, Electrocatalytic reduction-oxidation of chlorinated phenols using a nanostructured Pd-Fe modified graphene catalyst, Electrochim. Acta, 178 (2015) 92–100.
[28] H. Setiyanto, F.M. Sari, M.Y. Azis, R.S. Rahayu, A. Sulaeman, M.A. Zulfikar, D. Ratnaningrum, V. Saraswaty, Electrochemical degradation of methylene blue using Ce(IV) ionic mediator in the presence of Ag(I) ion catalyst for environmental remediation, 51 (2021) 149–159.
[29] R.V. McQuillan, G.W. Stevens, K.A. Mumford, Electrochemical removal of naphthalene from contaminated waters using carbon electrodes, and viability for environmental deployment, J. Hazard. Mater., 383 (2020) 121244, doi: 10.1016/j.jhazmat.2019.121244.
[30] K. Tian, K. Baskaran, A. Tiwari, Nonenzymatic glucose sensing using metal oxides–comparison of CuO, Co_3O_4, and NiO, Vacuum, 155 (2018) 696–701.
[31] G. Manjari, S. Saran, T. Arun, A.V. Rao, S.P. Devipriya, Catalytic and recyclability properties of phytogenic copper oxide nanoparticles derived from *Aglaia elaeagnoidea* flower extract, J. Saudi Chem. Soc., 21 (2017) 610–618.
[32] Z. Ma, Cobalt oxide catalysts for environmental remediation, Curr. Catal., 3 (2014) 15–26.
[33] A. Haider, M. Ijaz, S. Ali, J. Haider, M. Imran, H. Majeed, I. Shahzadi, M.M. Ali, J.A. Khan, M. Ikram, Green synthesized phytochemically (*Zingiber officinale* and *Allium sativum*) reduced nickel oxide nanoparticles confirmed bactericidal and catalytic potential, Nanoscale Res. Lett., 15 (2020) 50, doi: 10.1186/s11671-020-3283-5.
[34] F.K. Tan, J. Hassan, Z.A. Wahab, Electrical conductivity and dielectric studies of MnO_2 doped V_2O_5, Results Phys., 6 (2016) 420–427.
[35] M. Rasouli, H. Atashi, D. Mohebbi-Kalhori, N. Yaghobi, Bifunctional Pt/Fe-ZSM-5 catalyst for xylene isomerization, J. Taiwan Inst. Chem. Eng., 78 (2017) 438–446.
[36] Z.H. He, N. Li, K. Wang, W.T. Wang, Z.T. Liu, Selective hydrogenation of quinolines over a CoCu bimetallic catalyst at low temperature, J. Mol. Catal. B: Enzym., 470 (2019) 120–126.
[37] S.P. Kamble, V.D. Mote, Optical and room-temperature ferromagnetic properties of Ni-doped CuO nanocrystals prepared via auto-combustion method, J. Mater. Sci.: Mater. Electron., 32 (2021) 5309–5315.
[38] P. Viswanathan, K. Wang, J. Li, J.D. Hong, Multicore–shell Ag–CuO networked with CuO nanorods for enhanced non-enzymatic glucose detection, Colloids Surf., A, 598 (2020) 124816, doi: 10.1016/j.colsurfa.2020.124816.
[39] L. Barrientos, S. Rodriguez-Llamazares, J. Merchani, P. Jara, N. Yutronic, V. Lavayen, Unveiling the structure of Ni/Ni oxide nanoparticles system, J. Chil. Chem. Soc., 54 (2009) 391–393.
[40] N. Rahemi, M. Haghighi, A.A. Babaluo, S. Allahyari, M.F. Jafari, Syngas production from reforming of greenhouse gases CH_4/CO_2 over Ni–Cu/Al_2O_3 nanocatalyst: impregnated vs. plasma-treated catalyst, Energy Convers. Manage., 84 (2014) 50–59.
[41] M.P. Srinivasan, N. Punithavelan, Structural, morphological and dielectric investigations on NiO/CuO/ZnO combined semiconductor metal oxide structures based ternary nanocomposites, Mater. Res. Express, 5 (2018) 075033, doi: 10.1088/2053-1591/aad079.
[42] R.T. Rasheed, H.S. Mansoor, A.S. Mansoor, New colorimetric method to determine catalase mimic activity, Mater. Res. Express, 7 (2020) 025405, doi: 10.1088/2053-1591/ab706b.
[43] H. Jiang, L. Yang, C. Li, C. Yan, P.S. Lee, J. Ma, High–rate electrochemical capacitors from highly graphitic carbon–tipped manganese oxide/mesoporous carbon/manganese oxide hybrid nanowires, Energy Environ. Sci., 4 (2011) 1813–1819.
[44] X. Zhang, J.G. Wang, H. Liu, H. Liu, B. Wei, Facile synthesis of V_2O_5 hollow spheres as advanced cathodes for high-performance lithium-ion batteries, Materials, 10 (2017) 77, doi: 10.3390/ma10010077.
[45] D.M. Alqahtani, C. Zequine, C.K. Ranaweera, K. Siam, P.K. Kahol, T.P. Poudel, S.R. Mishra, R.K. Gupta, Effect of metal ion substitution on electrochemical properties of cobalt oxide, J. Alloys Compd., 771 (2019) 951–959.
[46] H.M. Robert, D. Usha, M. Amalanathan, R.R.J. Geetha, M.S.M. Mary, Spectroscopic (IR, Raman, UV, NMR) characterization and investigation of reactive properties of pyrazine-2-carboxamide by anti-bacterial, anti-mycobacterial, Fukui function, molecular docking and DFT calculations, Chem. Data Collect., 30 (2020) 100583, doi: 10.1016/j.cdc.2020.100583.
[47] U. Riaz, N. Singh, P. Kumar, Ultrasound-assisted synthesis of fluorescent oligomers of triphenylamine modified polyquinones: a comparison of experimental and computational spectral studies, J. Mol. Struct., 1217 (2020) 128374, doi: 10.1016/j.molstruc.2020.128374.
[48] T.F. Borgati, J.D.D. Souza Filho, A.B.D. Oliveira, A complete and unambiguous ^{1}H and ^{13}C-NMR signals assignment of para-naphthoquinones, ortho-and para-furanonaphthoquinones, J. Braz. Chem. Soc., 30 (2019) 1138–1149.
[49] J.W. Daniel, H. Bratt, The absorption, metabolism and tissue distribution of di(2-ethylhexyl) phthalate in rats, Toxicology, 2 (1974) 51–65.
[50] M.R. Habib, M.R. Karim, Antimicrobial and cytotoxic activity of di-(2-ethylhexyl) phthalate and anhydrosophoradiol-3-acetate isolated from *Calotropis gigantea* (*Linn.*) flower, Mycobiology, 37 (2009) 31–36.
[51] G.N. Rao, P.M. Kumar, V.S. Dhandapani, T.R. Krishna, T. Hayashi, Constituents of *Cassia auriculata*, Fitoterapia, 71 (2000) 82–83.
[52] P. Amade, M. Mallea, N. Bouaicha, Isolation, structural identification and biological activity of two metabolites produced by *Penicillium olsonii* Bainier and Sartory, J. Antibiot., 47 (1994) 201–208.

[53] D. Jalil, N.A. Fakhre, Extraction, identification and determination of di-(2ethylhexyl) phthalate (DEHP) plasticizer in some stored blood samples bags using different spectroscopic techniques, Ibn AL-Haitham J. Pure Appl. Sci. Technol., 29 (2017) 155–170.
[54] Q. Du, L. Shen, L. Xiu, G. Jerz, P. Winterhalter, Di-2-ethylhexyl phthalate in the fruits of *Benincasa hispida*, Food Addit. Contam., 23 (2006) 552–555.
[55] R. Pournejati, R. Gust, J. Sagasser, B. Kircher, K. Jöhrer, M.M. Ghanbari, H.R. Karbalaei-Heidari, In vitro evaluation of cytotoxic effects of di(2-ethylhexyl) phthalate (DEHP) produced by *Bacillus velezensis* strain RP137 isolated from Persian Gulf, Toxicol. in Vitro, 73 (2021) 105148, doi: 10.1016/j.tiv.2021.105148.
[56] M.M. Lotfy, H.M. Hassan, M.H. Hetta, A.O. El-Gendy, R. Mohammed, Di-(2-ethylhexyl) phthalate, a major bioactive metabolite with antimicrobial and cytotoxic activity isolated from River Nile derived fungus *Aspergillus awamori*, Beni-Seuf Univ. J. Basic Appl. Sci., 7 (2018) 263–269.
[57] D. Jalil, N.A. Fakhre, Extraction, identification and determination of di-(2ethylhexyl) phthalate (DEHP) plasticizer in some stored blood samples bags using different spectroscopic techniques, Ibn AL-Haitham J. Pure Appl. Sci. Technol., 29 (2017) 155–170.
[58] U.M. Sani, U.U. Pateh, Isolation of 1, 2-benzenedicarboxylic acid bis (2-ethylhexyl) ester from methanol extract of the variety minor seeds of *Ricinus communis* Linn. (*Euphorbiaceae*), Nig. J. Pharm. Sci., 8 (2009) 107–114.
[59] H. Shen, L. Ying, Y. Cao, G. Pan, L. Zhou, Simultaneous determination of phthalates and parabens in cosmetic products by gas chromatography/mass spectrometry coupled with solid phase extraction, Chin. J. Chromatogr. (Se Pu), 25 (2007) 272–275.
[60] Y. Kudo, K. Obayashi, H. Yanagisawa, F. Maruyama, S. Fujimaki, H. Miyagawa, K. Nakagawa, Development of a screening method for phthalate esters in polymers using a quantitative database in combination with pyrolyzer/thermal desorption gas chromatography mass spectrometry, J. Chromatogr. A, 1602 (2019) 441–449.
[61] V.N. Kouloumbos, D.F. Tsipi, A.E. Hiskia, D. Nikolic, R.B. van Breemen, Identification of photocatalytic degradation products of diazinon in TiO_2 aqueous suspensions using GC/MS/MS and LC/MS with quadrupole time-of-flight mass spectrometry, J. Am. Soc. Mass Spectrom., 14 (2003) 803–817.